Spin-orbit state-selected reactions of $Kr^+(^2P_{3/2}$ and $^2P_{1/2})$ with H_2, D_2, and HD from thermal energies to 20 eV c.m.

Kent M. Ervin and P. B. Armentrout[a)]
Department of Chemistry, University of California at Berkeley, Berkeley, California 94720

(Received 30 June 1986; accepted 12 August 1986)

Spin-orbit state-selected reactions of $Kr^+(^2P_J)$, $J = 3/2$ and $J = 1/2$, with isotopic molecular hydrogen (H_2, D_2, and HD) to form KrH^+ and KrD^+ are investigated using guided ion beam techniques. Reaction cross sections for each spin-orbit state are measured as a function of the relative translational energy of the reactants from near thermal energies up to 20 eV c.m. At low energies, the cross sections for reaction with H_2 and D_2 are each about 2.6 times larger for the $^2P_{3/2}$ ground spin-orbit state of krypton ion than for the $^2P_{1/2}$ excited state. For the HD reaction, the $^2P_{3/2}$ reactivity is enhanced by a factor of about 4.2. A higher-energy process, which exhibits an apparent activation energy of about 1 eV, is present *only* for the $^2P_{3/2}$ spin-orbit state. The $Kr^+(^2P_{3/2})$ spin-orbit state exhibits a strong intermolecular isotope effect, showing the unusual dependence $\sigma(HD) > \sigma(H_2) > \sigma(D_2)$ for the total reaction cross sections at low energies. Cross sections for the $Kr^+(^2P_{1/2})$ state show a much smaller dependence on the hydrogen isotope. The intramolecular isotope effect for the individual KrH^+ and KrD^+ channels in the reaction with HD shows several reversals over the energy range studied. These results are discussed in terms of the potential energy surfaces of the krypton–hydrogen system.

INTRODUCTION

Considerations of electronic structure are basic to the understanding of chemical reactivity. Whether approached from a simple molecular orbital viewpoint or by high-level *ab initio* calculations of potential energy hypersurfaces, determining the evolution of the electronic interactions along the reaction path is essential to the prediction and explanation of reaction kinetics and dynamics. Much progress has been made in understanding these effects in chemical reactions, including the role of multiple electronic potential energy surfaces.[1]

Spin-orbit coupling, a more subtle aspect of electronic structure, is often neglected in such considerations. However, a growing body of experimental investigation into the effects of the spin-orbit state of reactant atoms on chemical reactivity shows that spin-orbit effects can be quite pronounced. Investigations in the last decade have shown substantial differences in reactivity for the spin-orbit states of halogen atoms ($^2P_{3/2}$ and $^2P_{1/2}$).[2–8] Investigations of Sn($^3P_0$ and $^3P_1$)[9] and Hg($^3P_0$ and $^3P_2$)[10] have shown that the higher spin-orbit levels of these metal atoms tend to be significantly more reactive. The reactions of metastable ^3P_J excited states of Ar, Kr, and Xe with small halogen containing molecules have been studied.[11] Dagdigian and co-workers[12] have recently used an optical pumping method to study selected spin-orbit states of Ca(^3P_J, $J = 0,1,2$) reacting with Cl_2, Br_2, and alkyl halides. They observe a substantial spin-orbit state dependence for the chemiluminescent reaction channels (formation of *A* CaX and *B* CaX, X = Cl or Br), with the higher spin-orbit levels generally showing greater reactivity. The ground state product channel, however, exhibits an inverse spin-orbit effect for reaction with Cl_2.[12]

In the field of ion–molecule chemistry, a number of reactions of spin-orbit state-selected rare gas ions have been studied. The charge transfer reactions of $Xe^+(^2P_J)$ with Xe and O_2[13] and of $Ar^+(^2P_J)$ with N_2[14–17] and CO[16] have been examined. Photoionization measurements by Chupka[18] and threshold-electron secondary-ion coincidence studies by Koyano and co-workers[19] have shown that the $^2P_{1/2}$(0.17 eV)[20] excited spin-orbit level of Ar^+ reacts 30% to 50% faster with H_2 than does the $^2P_{3/2}$ (0.0 eV) ground state. Ion cyclotron resonance,[21] selected ion flow tube,[22] and drift tube[23] techniques have been used to study thermal reaction rates of spin-orbit state-selected $Kr^+(^2P_J)$ and $Xe^+(^2P_J)$ with a number of small molecules. In contrast to the $Ar^+ + H_2$ result, these studies show that exothermic reactions of the ground $^2P_{3/2}$ spin-orbit levels of Kr^+ and Xe^+ react at least as fast and in many cases much faster than the excited $^2P_{1/2}$ spin-orbit levels. This inverse spin-orbit effect occurs despite the substantially higher energy of the upper state (0.67 eV for Kr^+ and 1.31 eV for Xe^+).[20]

This work presents measurements of spin-orbit state-selected cross sections for the reactions of krypton (1 +) ions with isotopic molecular hydrogen:

$$Kr^+(^2P_J) + H_2 \rightarrow KrH^+ + H, \quad (1)$$

$$Kr^+(^2P_J) + D_2 \rightarrow KrD^+ + D, \quad (2)$$

$$Kr^+(^2P_J) + HD \rightarrow KrH^+ + D \quad (3a)$$

$$\rightarrow KrD^+ + H. \quad (3b)$$

Guided ion beam techniques are used to study the reactions from near thermal energies to relative collision energies of 20 eV c.m. Reaction (1) has an exothermicity of $\Delta H^\circ_0 = -0.29 \pm 0.06$ eV for the $^2P_{3/2}$ ground spin-orbit state of krypton ions and $\Delta H^\circ_0 = -0.96 \pm 0.06$ eV for the $^2P_{1/2}$ excited spin-orbit state.[24] This large difference in energetics alone suggests that spin-orbit effects could be important in reactions (1) through (3). In a recent article,[25] we investigated the analogous reactions of argon(1 +) ions us-

[a)] N. S. F. Presidential Young Investigator 1984–1989; Alfred P. Sloan Fellow 1986–1988.

 0021-9606/86/236380-16$02.10

ing guided beam techniques. Spin-orbit state selection was not attempted in the argon studies because the relatively small spin-orbit splitting in Ar^+ (0.17 eV) makes it experimentally difficult to state-select reactants. The larger splitting in Kr^+ (0.67 eV) enables the straightforward use of state-specific ion–molecule reactions[21,22] to produce ion beams of a particular $Kr^+(^2P_J)$ spin-orbit state.

Previous measurements of spin-orbit state-specific rates of reaction (1) at thermal energies have shown that the $^2P_{3/2}$ ground state reacts significantly faster than $^2P_{1/2}$ excited state.[21,22,26] Table I lists measured rate constants for individual spin-orbit states. Chupka[26] observed in photoionization experiments that the ratio of rates $k(^2P_{3/2})/k(^2P_{1/2})$ is ~ 2.5 for reaction (1). In rate constant measurements, Futrell and co-workers[21] obtained a value of 1.6 and Adams, Smith, and Alge (ASA)[22] obtained ~ 1.9. For reactions (2) and (3), ASA found larger spin-orbit effects (see Table I). It is somewhat surprising that the upper spin-orbit state reacts less efficiently at thermal energies despite the larger exothermicity for forming $KrH^+ + H$ products. This result is opposite to the spin-orbit state dependence of reactions of $Ar^+(^2P_J)$ with H_2 and D_2.[19,27]

Other previous experimental investigations of reactions (1), (2), and (3) have used a statistical mixture of krypton ion spin-orbit states, i.e., $^2P_{3/2}$:$^2P_{1/2} \approx 2$:1. These studies find that the observed rate for reaction (1) is only 10%–16% of the collision rate predicted by the Langevin–Gioumousis–Stevenson (LGS) model[28] for charge-induced dipole interactions (see Table I). This means that despite the exothermicity of the reaction, the probability of reaction per collision is rather small. This contrasts with the $Ar^+ + H_2$ reaction, which is more exothermic, $\Delta H^\circ_0 = -1.5$ eV, and has a rate about two-thirds of the LGS collision rate at thermal energies.[25]

The *intermolecular* isotope effect at thermal energies differs substantially for the argon and krypton systems. Observations[25] for Ar^+ in good accord with the LGS collision model, which predicts that $k(H_2) > k(HD) > k(D_2)$ due to mass effects. In the Kr^+ system, however, Bowers and co-workers[29] find an unusual intermolecular kinetic isotope effect in the rate constants from 100 to 400 K, namely $k(HD) > k(H_2) > k(D_2)$. This result has been reproduced qualitatively by Adams, Smith, and Alge[22] (Table I).

Hierl and co-workers[30] measured the reaction cross sections at hyperthermal energies, from 0.036 to 3 eV for reaction (1) and from 0.08 to 3.1 eV for reaction (3). The total reaction cross sections have approximately the $E^{-1/2}$ energy dependence predicted by the LGS collision cross section at the lower energies, but with only 10% to 20% of its magnitude.[30] The angular and velocity distributions of products for reaction with H_2,[30] D_2,[31] and HD[30] show that the reactive scattering at low energies is isotropic about the center-of-mass velocity of the system. This was interpreted[30] as indicating a mechanism in which low impact parameter collisions give hard sphere-like scattering of the ionic product and substantial momentum transfer to the neutral product. A preference for low impact parameter collisions is also consistent with the low reaction rate. At larger energies (2–3 eV), the ionic products are more forward scattered, indicative of a more direct, impulsive reaction mechanism, but there is still substantial wide-angle scattering.

The *intramolecular* isotope effect for reactions (3a) and

TABLE I. Thermal reaction rate constants.[a]

Reactant	$Kr^+(^2P_J)$[b]	$Kr^+(^2P_{3/2})$	$Kr^+(^2P_{1/2})$	$k(^2P_{3/2})/k(^2P_{1/2})$	Reference
H_2	2.3 ± 0.6	2.8 ± 0.7	1.1 ± 0.3	2.6	this work
	2.4 ± 0.7[c]	2.8 ± 0.6	1.5 ± 0.3	1.9	22
	1.8 ± 0.2				29
	1.7 ± 0.2	1.9 ± 0.2	1.2 ± 0.4	1.6	21
		2.0 ± 0.7[d]			49
	1.5 ± 0.3				52
				2.5	26
	15.0	15.0	15.0		LGS[e]
D_2	1.4 ± 0.4	1.7 ± 0.5	0.67 ± 0.2	2.6	this work
	2.2 ± 0.4[c]	2.8 ± 0.6	0.89 ± 0.2	3.1	22
	0.9 ± 0.2				29
	1.3 ± 0.2				21
		1.5 ± 0.5[d]			49
	10.7	10.7	10.7		LGS[e]
HD[f]	3.2 ± 0.7	4.3 ± 1	1.0 ± 0.3	4.2	this work
	5.1 ± 1[c]	7.3 ± 1.5	0.78 ± 0.2	9.4	22
	2.8 ± 0.3				29
	12.3	12.3	12.3		LGS[e]

[a] All rates at 300 K in units of 10^{-10} cm^3 s^{-1}; relative uncertainties cited by the original authors have been converted to absolute error limits.
[b] Statistical population of spin-orbit states ($^2P_{3/2}$: $^2P_{1/2} \approx 2:1$).
[c] Weighted average of results for $^2P_{3/2}$ and $^2P_{1/2}$.
[d] Approximately 90% $^2P_{3/2}$.
[e] Langevin–Gioumousis–Stevenson collision rate (Ref. 28).
[f] Sum of KrH^+ and KrD^+ channels.

(3b) at hyperthermal energies also exhibits quite unusual behavior. Hierl and co-workers[30] observed that the product branching ratio varied from 50% KrH^+ at their lowest ion energy ($\sim$0.08 eV c.m.) to a maximum of about 70% KrH^+ at 0.7 eV c.m. and back down to 20% KrH^+ at 3 eV c.m. The HD intramolecular isotope effect was explained using an orientational model for low-energy reactions[32] and a collinear reaction model at the higher energies.[30]

A high energy feature in the cross sections of Kr^+ with H_2, D_2, and HD was observed in work reported by Klein.[33] Contrary to the typical behavior for exothermic ion–molecule reactions of a monotonic decline with increasing translational energy, the cross sections increase after an initial decline and peak at higher energies. This is suggestive of a second reaction mechanism or reaction channel with an activation barrier.

The spin-orbit effects and unusual inter- and intramolecular isotope effects observed in these previous studies indicate that the $Kr^+ + H_2$ reaction system is quite complex. Unfortunately, an overall understanding of the underlying reaction dynamics has not emerged. This investigation was initiated in hopes that a comprehensive study of both spin-orbit effects and isotope effects over a wide translational energy range would lead towards such an understanding. The results are discussed in terms of adiabatic and nonadiabatic couplings between low-lying electronic potential energy surfaces of the system.

EXPERIMENTAL METHODS

Guided ion beam methods are used to measure the integral cross sections of reactions (1), (2), (3a), and (3b) from thermal energies up to ion energies of several hundred electron volts. The guided ion beam apparatus and data reduction procedures were described in detail in conjunction with our investigation of the $Ar^+ + H_2$ reaction.[25] A brief outline of the experimental technique is included here along with a description of the method of producing spin-orbit state-selected beams of $Kr^+(^2P_J)$ ions.

Guided ion beam apparatus

The guided ion beam apparatus is a significantly improved version of conventional ion beam/gas cell instruments used to measure total reaction cross sections. Ions are extracted from the ion source, described below, focused into a beam, and mass analyzed in a magnetic sector to select the desired species. The ions are then refocused and injected at the desired ion kinetic energy into a radio-frequency octopole ion beam guide. The octopole, which passes through the gas collision cell, creates a radial potential well along the axis of the ion beam which traps ions in radial directions but does not affect their axial velocities. This trapping field serves to collect product ions scattered in all directions with near 100% efficiency. This greatly improves the sensitivity compared to conventional beam/gas cell instruments and avoids artifacts due to different collection efficiencies for product ions scattered in different directions. The octopole also allows operation of the ion beam at very low energies (down to 0.1 eV lab), where the beam would become dispersed without the trapping field due to space charge effects and focusing aberrations.

Neutral reactant densities are kept low enough that multiple ion–molecule collisions are improbable. Product ions and unreacted primary ions drift to the end of the octopole, are extracted from it, mass analyzed with a quadrupole mass filter, and detected by secondary electron scintillation and pulse counting electronics. The reaction cross sections are derived directly from the reactant and product ion intensities, the gas cell pressure, and the estimated reaction path length.[25] The relative uncertainty of the cross sections at different energies and for different reactions is within 5% for cross sections greater than 1×10^{-17} cm^2 and is limited by statistical counting uncertainties for smaller cross sections. The uncertainty in the absolute magnitude of the cross sections is limited mainly by the gas pressure measurement and by the estimate of the reaction path length. We estimate that the error in the absolute cross sections from all sources is $\pm$ 20%.

Ion sources

Two different ion sources are used in these experiments. The first is a conventional low-pressure electron impact ionization source, which has been described previously.[25] Adams, Smith, and Alge[22] have shown that low-pressure electron impact ionization produces a statistical mixture of $Kr^+(^2P_J)$, i.e., an ion beam with twice as much $^2P_{3/2}$ ground state as $^2P_{1/2}$ excited state, and the present experiments confirm this (see below). The electron energies are kept below 27.5 eV, the threshold for forming higher excited states of Kr^+.

Ion beams with enhanced populations of one of the spin-orbit states are produced using a high pressure coaxial ion source. This source is modeled after the design of Bowers and co-workers[34] and is described in detail elsewhere.[35] Electrons from a filament or ions from a separate electron impact ion source are injected into a 2 cm long drift region which contains a relatively high pressure (50 to 500 mTorr) of a reactant gas or gas mixture. In the case of injecting electrons, ions are formed by electron impact inside the drift cell. The ions undergo numerous collisions with the bath gas while being drawn through the cell by a weak electric field (1 to 5 V cm^{-1}) towards an exit aperture. The collisions serve to thermalize the ions translationally. The reactant gas mixtures may be varied to utilize ion–molecule reaction sequences which produce the desired ion species.

$Kr^+(^2P_J)$ spin-orbit state selection

Several groups have reported the use of state-specific ion–molecule reactions to produce spin-orbit state-selected $Kr^+(^2P_J)$ ions.[21–23,26] These methods take advantage of large differences in the thermal reaction rates of the $^2P_{3/2}$ and $^2P_{1/2}$ states with various reactant gases. We use appropriate reactions both to produce ions in a selected spin-orbit state and to diagnose the spin-orbit population of the ion beam. The specific reactions used for these purposes are discussed next.

To produce ion beams of primarily $Kr^+(^2P_{3/2})$, mixtures of Kr and CO are used in the drift cell. Ions are made by

injecting electrons into the drift cell with electron energies of less than 35 eV. Following electron impact ionization of either Kr or CO, the ions are thermalized by collisions and undergo the following charge transfer processes:

$$Kr^+(^2P_{3/2}) + CO \underset{k_{-4}}{\overset{k_4}{\rightleftarrows}} CO^+ + Kr - 0.014\ eV, \quad (4)$$

$$Kr^+(^2P_{1/2}) + CO \xrightarrow{k_5} CO^+ + Kr + 0.66\ eV. \quad (5)$$

The forward and reverse rates of the near-resonant charge transfer process with ground state Kr^+ are $k_4 = 2.0\times10^{-10}$ and $k_{-4} = 5.1\times10^{-10}$, respectively, while the nonresonant charge transfer with the $^2P_{1/2}$ krypton ions is slow, $k_5 = 2.8\times10^{-11}$ (all rates in units of $cm^3\ s^{-1}$ and at 300 K).[22] Since the reverse of reaction (5) is endothermic, it does not occur under the drift cell conditions. The fast rate coefficient k_{-4} ensures that the equilibrium mixture of Kr^+ ions produced will be greatly enhanced in the $^2P_{3/2}$ ground spin-orbit state. Also, sufficient collisions occur for reaction (5) to deplete the $^2P_{1/2}$ ions formed initially by electron impact.

To produce ion beams consisting primarily of the $Kr^+(^2P_{1/2})$ excited spin-orbit state, we take advantage of the very large difference in rates of the spin-orbit states for charge transfer with nitrous oxide:

$$Kr^+(^2P_J) + N_2O \rightarrow N_2O^+ + Kr. \quad (6)$$

The rates constants[22] are $k_6(^2P_{3/2}) = 4.0\times10^{-10}$ and $k_6(^2P_{1/2}) = 1.5\times10^{-11}$. In mixtures of Kr and N_2O in the drift cell, the $^2P_{3/2}$ state of Kr^+ is depleted rapidly by reaction (6), while the $^2P_{1/2}$ spin-orbit state reacts away at a much slower rate. This results in ion beams with predominantly $Kr^+(^2P_{1/2})$.

In some of the experiments, Kr^+ ions produced by electron impact were injected into the drift cell containing CO or N_2O (rather than injecting electrons into the drift cell containing a mixture of Kr and the reactant gas). Collisions with the reactant gas thermalize the ions translationally and reactions (4), (5), and (6) determine the final spin-orbit state population of the ions extracted from the drift cell. Either method—injection of ions or of electrons—gives similar spin-orbit state selectivity.

Spin-orbit state determination

In order to determine the spin-orbit state population of the Kr^+ beam, diagnostic reactions are measured in the reaction cell of the beam guide apparatus. The reactions of $Kr^+(^2P_J)$ with methane[21,22,36] are particularly useful for this purpose:

$$Kr^+(^2P_{3/2}) + CH_4 \rightarrow CH_4^+ + Kr + 1.3\ eV, \quad k = 1.0\times10^{-10}, \quad (7)$$

$$Kr^+(^2P_{1/2}) + CH_4 \rightarrow CH_4^+ + Kr + 2.0\ eV, \quad k = 0.1\times10^{-10} \quad (8a)$$

$$\rightarrow CH_3^+ + H + Kr + 0.3\ eV, \quad k = 0.9\times10^{-10}. \quad (8b)$$

The reaction of the $^2P_{3/2}$ state to form CH_3^+ is endothermic by about 0.4 eV, so that process is not allowed at low energies. Other reaction channels, formation of KrH^+, $KrCH_2^+$, and $KrCH_3^+$, have much smaller cross sections and can be neglected.[37] Based on the above reaction rates,[22] the fraction f_J of the spin-orbit state $Kr^+(^2P_J)$ can be determined from the product ion intensities $I(CH_3^+)$ and $I(CH_4^+)$ according to the formula

$$f_{1/2} = 1 - f_{3/2} = I(CH_3^+)/0.9[I(CH_3^+) + I(CH_4^+)]. \quad (9)$$

The reaction rates used to derive formula (9) apply to thermal conditions at 300 K; however, measurements of the cross sections for reactions (7) and (8) in this lab show the value obtained from formula (9) is independent of energy from thermal energies up to 0.2 eV. This is because the energy dependence of reaction (7) is very similar to that of the total cross section for reaction (8) and because the branching ratio for reactions (8a) and (8b) is constant over this energy range.[38] At higher energies, the endothermic formation of CH_3^+ from $Kr^+(^2P_{3/2})$ alters these relationships. In routine determinations of the Kr^+ ion beam spin-orbit state populations for these experiments, the CH_3^+ and CH_4^+ product intensities are measured at 0.10 eV c.m. (0.64 eV lab). This energy is well below the ~0.4 eV threshold for formation of CH_3^+ from $Kr^+(^2P_{3/2})$. A complicating aspect in the measurement of the CH_3^+/CH_4^+ branching ratio is the occurrence of the rapid secondary reactions $CH_4^+ + CH_4 \rightarrow CH_5^+ + CH_3^+$ and $CH_3^+ + CH_4 \rightarrow C_2H_5^+ + H_2$. Ambiguities due to these processes are avoided by measuring the CH_4^+ and CH_3^+ product intensities at a number of methane pressures (0.02 to 0.3 mTorr in the reaction cell) and extrapolating to zero pressure.

The spin-orbit state determination verifies that the low pressure electron impact source with an electron energy of 28 eV or less produces a statistical population of spin-orbit states. In 12 measurements over the course of about a year, the spin-orbit population determined by the procedure described above gave the average value $f_{3/2} = 0.684$, with a standard deviation of 0.026. This is in good agreement with the expected value for a statistical population of $f_{3/2} = 0.667$. The standard deviation gives an indication of the uncertainty of the procedure, namely 2%–3%, although some of the apparent run-to-run deviation may be real.

The drift cell ion source conditions are optimized to produce the desired spin-orbit state of Kr^+ by monitoring the CH_3^+/CH_4^+ product ratio for reaction with CH_4. The conditions which may be varied are the total pressure in the ion source drift region, the relative pressures of reactant gases, the electron or ion injection energy, and the electric field in the drift region. It has proven possible to make $Kr^+(^2P_J)$ ion beams of better than 95% purity of either spin-orbit state. Before and after each measurement of the cross sections for reactions (1) through (3), the CH_3^+/CH_4^+

branching ratio for reaction with methane at 0.1 eV c.m. is measured to determine the spin-orbit state population. If the spin-orbit state population according to formula (9) changed during the course of an experiment by more than two or three percentage units, that set of results was discarded. That situation ocurred rarely, however, and could be attributed to changes in the ion source pressures or other source conditions.

The accuracy of the state population determinations is substantiated by the self-consistency of the results for reactions (1) through (3) with different initial state populations. The cross sections (see Results section) at a given energy depend linearly on the measured state populations, as must be the case for a two-component mixture of ions. The cross section data at each relative energy for three or four different spin-orbit state mixtures are extrapolated to obtain cross sections for the pure $^2P_{3/2}$ and $^2P_{1/2}$ reactant ions. However, since we are able to make ion beams of greater than 95% spin-orbit state purity, the extrapolations make relatively small corrections to the spin-orbit effects which are apparent in the raw data for the nearly pure $Kr^+(^2P_J)$ beams.

Isotopic reactants

Commercially supplied H_2 and D_2, 99.99% purity, is used. HD gas has been synthesized by standard methods.[39] Its purity was confirmed by mass spectrometric and by Raman spectroscopic analyses. The HD is greater than 96% pure, with approximately equal amounts of H_2 and D_2 impurities.

The initial magnetic mass spectrometer on the ion beam guide apparatus[25] has limited mass resolution and passes small amounts of krypton isotopes other than the desired one. In order to avoid problems with isotopic overlap with hydride and deuteride products, the highest-mass stable krypton isotope, ^{86}Kr (17.4% natural abundance), is used in all of the experiments reported here.

Interaction energies

The absolute kinetic energy of the ion beam is measured to within ± 0.10 eV lab [± 2.3, ± 4.5, and ± 3.4 meV c.m. for reactions (1), (2), and (3), respectively] by utilizing the octopole itself as a retarding energy analyzer.[25] The ion beam energy and its distribution is determined by fitting a Gaussian distribution to the retarding energy curve. The ion sources described above produce ion beams with typical energy spreads of 0.2 full width at half-maximum.

The laboratory ion energies, E_{lab}, are converted to nominal center-of-mass frame energies, $E_{c.m.}$, via the usual stationary target assumption[25]:

$$E_{c.m.} = E_{lab} \cdot m/(M+m), \tag{10}$$

where M is the ion mass and m is the target molecule mass. The range of energies accessible to the beam guide apparatus is $E_{lab} = 0.1$ to 800 eV. The thermal motion of the hydrogen target molecules creates a distribution of relative interaction energies for each nominal center-of-mass energy $E_{c.m.}$.[25,40] The mean relative energy of this distribution is given by

$$\langle E \rangle = E_{c.m.} + (3/2)\gamma k_B T, \tag{11}$$

where $\gamma = M/(M+m)$ and T is the target gas temperature (305 K). The energy distribution approaches a Boltzmann distribution at very low ion energies, with an effective temperature $T_{eff} = \gamma T$. With increasing ion energy, the width of the distribution increases as $E^{1/2}$, but becomes much narrower than a thermal Boltzmann distribution with the same mean energy. The spread in the ion beam energy is generally negligible in comparison to the energy spread caused by the target gas motion. The effect of the relative energy distributions on the apparent cross sections of exothermic reactions is described in more detail in our report on the $Ar^+ + H_2$ reaction.[25]

RESULTS

Statistical $Kr^+(^2P)$ cross sections

Results using a $Kr^+(^2P_J)$ ion beam with a statistical mixture of spin-orbit states, $^2P_{3/2}$:$^2P_{1/2} \approx 2$:1, will be presented first in order to point out the major features of the excitation functions and to compare the present work with previous results. In the following discussion, we will use the notation $Kr^+(^2P)$, i.e., without the subscript J, to designate krypton ion beams with a statistical population of spin-orbit levels.

$Kr^+(^2P) + H_2$

The cross section for reaction (1) with a statistical population of krypton ion spin-orbit states is presented in Fig. 1.

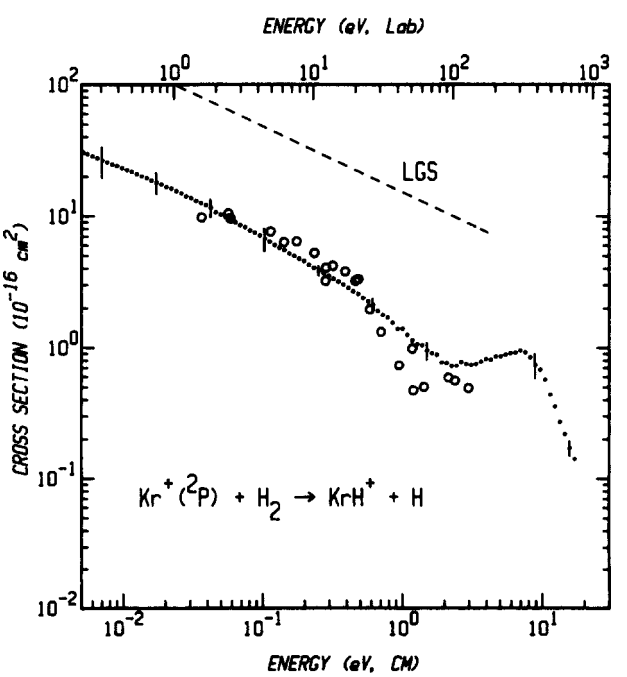

FIG. 1. Cross section for reaction (1) with a statistical mixture of $Kr^+(^2P_J)$ spin-orbit states. The present results (small points) are plotted as a function of the ion kinetic energy in the laboratory frame (upper scale) and the center-of-mass frame (lower scale). Each point represents an average of several determinations. The vertical error bars indicate ± 2 standard deviations. The large open circles reproduce the data of Hierl and coworkers (Ref. 30). The broken line gives the collision cross section predicted by the LGS model.

The plot shows the cross section vs the laboratory ion energy and the center-of-mass frame energy in electron volts. Unless noted otherwise, all further references to energy are to the center-of-mass frame energy. The data shown represent averages of several measurements made over a period of months. Vertical error bars show ± 2 standard deviation of all of the averaged results and thus indicate the reproducibility of the measurements. The experimental uncertainty of the absolute magnitude of the cross section is $\pm 20\%$. Similar uncertainties apply to all of the cross section results.

At energies below about 0.5 eV, the cross section (Fig. 1) varies with collision energy approximately as $E^{-0.5}$, as predicted by the LGS model for the orbiting collision cross section for an ion-induced dipole potential.[28] However, the magnitude is about seven times smaller than the LGS cross section (Fig. 1). From about 0.5 eV up to about 1.5 eV, the cross section declines at a significantly faster rate with increasing energy, $\sigma \propto E^{-1.2\pm0.2}$. At higher energies, a second feature is evident. The cross section peaks at about 6 eV, then declines rapidly at higher energies.

Hierl and co-workers[30] measured the cross section for reaction (1) over the range of 0.04 to 3 eV. Their results are shown in Fig. 1 for comparison. The agreement in both magnitude and energy dependence is quite good considering the differences in instrumentation.[41] Our values are within the quoted 50% uncertainty of Hierl's data. Unpublished results of Klein[33] and Fennelly[42] also are in general agreement with the present results. The high energy feature of the cross section for this reaction and reactions (2) and (3) was first reported by Klein.[33]

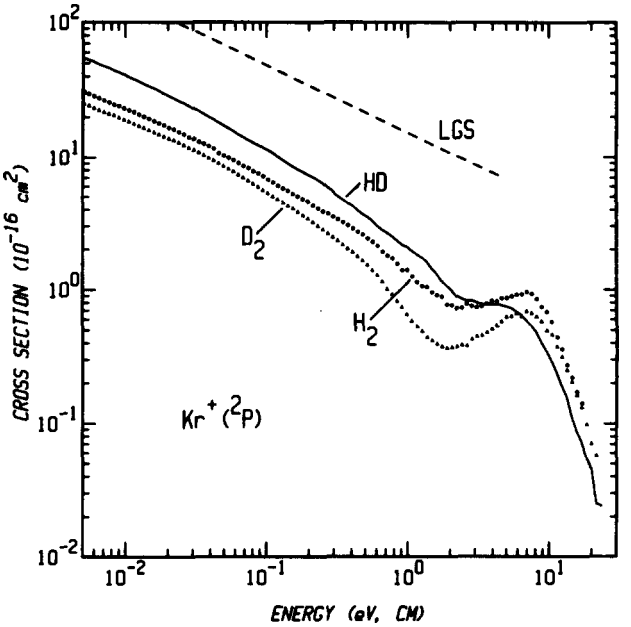

FIG. 2. Comparison of experimental cross sections for reactions (1), (2), and (3) with a statistical mixture of $Kr^+(^2P_j)$ spin-orbit states, plotted as a function of the ion kinetic energy in the center-of-mass frame. The solid line represents the sum of the KrH^+ and KrD^+ product channels for reaction (3). The broken line gives the collision cross section predicted by the LGS model.

$Kr^+(^2P) + H_2, D_2, HD$: Intermolecular Isotope effect

Figure 2 compares the total cross sections for $Kr^+(^2P)$ reacting with H_2, D_2, and HD. There are significant differences in the cross sections for the three isotopic reactants. The relative behavior of the cross sections at low energies is very similar, but the magnitudes differ. The ratio of cross sections $\sigma(H_2):\sigma(HD):\sigma(D_2)$, where $\sigma(HD)$ denotes the sum of the KrH^+ and KrD^+ channels of reaction (3), is approximately 1.0: 1.8: 0.8 below 0.1 eV. This result is counter to the usual expectation that the cross sections should be identical when compared on the center-of-mass energy scale. In the analogous reactions of argon ions, the cross sections are in fact identical within experimental uncertainty.[25] The ordering of the cross sections, $\sigma(HD) > \sigma(H_2) > \sigma(D_2)$, is also unusual and indicates that the intermolecular isotope effect is *not* simply a mass effect.

All three isotopic reactions exhibit the second feature at higher energies. The shape and magnitude of the high energy feature is very similar for reactions (1) and (2), but the feature has a different shape for reaction (3). This effect will be discussed further below.

For comparison with rate measurements of the intermolecular isotope effect, our low energy cross sections can be converted into thermal rate constants by integration over a Boltzmann distribution of translational energies. We have described the detailed procedure previously.[25] Comparison of rate constants derived from the guided ion beam cross sections for the $Ar^+ + H_2$ reaction with a number of other experimental determinations demonstrated that accurate thermal rate constants may be obtained by these methods.[25] The derived rate constants for 300 K are compared with literature results in Table I. The intermolecular isotope effect is given by the ratios of rate constants $k(H_2):k(HD):k(D_2) = 1.0:1.4:0.6$. In contrast, simple collision theory predicts ratios of 1.0:0.82:0.71 due to the mass effect on relative collision velocities (assuming identical cross sections). The present results agree well with the thermal rate constant measurements of Bowers and co-workers,[29] who obtain ratios of 1.0:1.6:0.50, and less well with Adams, Smith, and Alge (ASA),[22] who find 1.0:2.1:0.9. While the rate constants for reaction (1) obtained by all researchers are in good agreement (Table I), there are discrepancies for reactions (2) and (3). In particular, the rate constants obtained by ASA for reactions (2) and (3) are up to a factor of 2 higher than those obtained by us and by Bowers and co-workers.[28] Nevertheless, the unusual ordering of the intermolecular isotope effect is reproduced in all three experiments.

$Kr^+(^2P) + HD$: Intramolecular Isotope effect

The individual KrH^+ and KrD^+ product cross sections for reaction with HD are shown in Fig. 3. The intramolecular isotope effect is also presented in Fig. 4 as the branching ratio $\sigma(KrH^+)/[\sigma(KrH^+) + \sigma(KrD^+)]$, which illustrates the dramatic changes in the isotope effect as a function of energy. At the lowest energies, the reaction makes $\sim 46\%$ KrH^+, in very good agreement with the thermal rate constant measurements.[22,29] The isotope effect reverses at $E_{c.m.} \approx 0.030$ eV,[43] above which the KrH^+ product is favored.

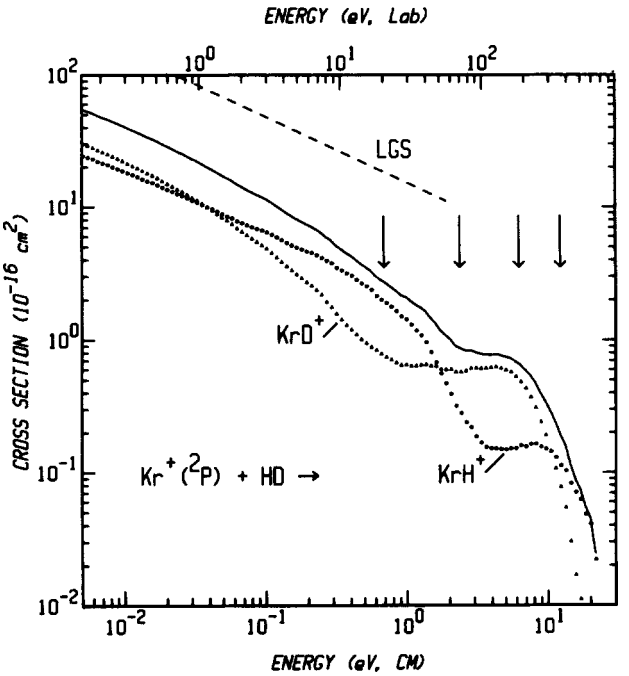

FIG. 3. Cross sections for the individual KrH^+ and KrD^+ product channels of reaction (3) with a statistical mixture of $Kr^+(^2P_J)$ spin-orbit states. The cross sections (small points) are plotted as a function of the ion kinetic energy in the laboratory frame (upper scale) and the center-of-mass frame (lower scale). The sum of the two channels is represented by the solid line. The broken line gives the collision cross section predicted by the LGS model. From left to right, the arrows indicate the apparent thresholds for the $^2P_{3/2}$ high energy feature for KrD^+ and KrH^+ and the spectator stripping model critical energies for KrD^+ and KrH^+ (Table II).

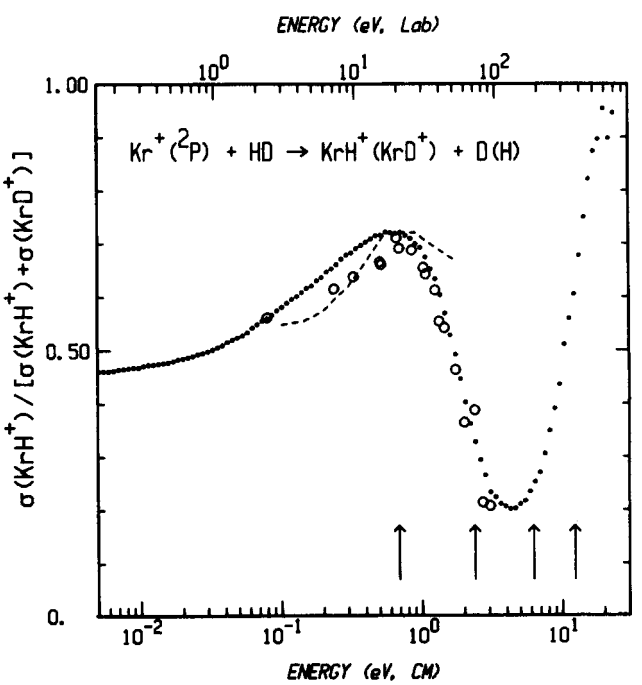

FIG. 4. Isotopic branching ratio for reaction (3) presented as the fraction of KrH^+ product. The experimental ratio (small points) is plotted as a function of the ion kinetic energy in the laboratory frame (upper scale) and the center-of-mass frame (lower scale). The large open circles are the data of Hierl and co-workers (Ref. 30). The dashed line is the prediction of the orientation isotope effect model (Ref. 32). From left to right, the arrows indicate the apparent thresholds for the $^2P_{3/2}$ high energy feature for KrD^+ and KrH^+ and the spectator stripping model critical energies for KrD^+ and KrH^+ (Table II).

The branching ratio peaks at 75% KrH^+ at about 0.6 eV, then falls again. In the region of the second feature of the total cross section, the branching undergoes further large swings, bottoming out at about 20% KrH^+ at 4 eV, then rising until KrH^+ predominates again above 10 eV.

Hierl and co-workers[30] measured the intramolecular isotope effect for reaction (3) over the energy range 0.08 to 3.1 eV. Their results are plotted in Fig. 4 for comparison with the present data. The agreement is excellent. Unpublished results of Klein[33] and Fennelly *et al.*[42] are also in general agreement with the present data.

Spin-orbit state-selected $Kr^+(^2P_J)$ cross sections

Figure 5 displays the spin-orbit state dependence of the cross sections of reaction (1). The raw data (lines) are shown for $Kr^+(^2P_J)$ ion beams with spin-orbit state populations of 96.4 $\pm$ 2% $^2P_{3/2}$ and 95.4 $\pm$ 2% $^2P_{1/2}$ as well as a statistical mixture. The points represent these data and two other runs extrapolated to pure spin-orbit states at each energy. Figure 5 demonstrates that the extrapolations make rather minor corrections to the large spin-orbit effect already apparent in the raw data. The extrapolations have a somewhat higher uncertainty in regions where one spin-orbit state is much less reactive than the other.

Figures 6 and 7 show the spin-orbit state-selected cross sections for reactions (2) and (3). For these, only the extrapolated cross sections are shown. The quality of the raw data is similar to that shown in Fig. 5.

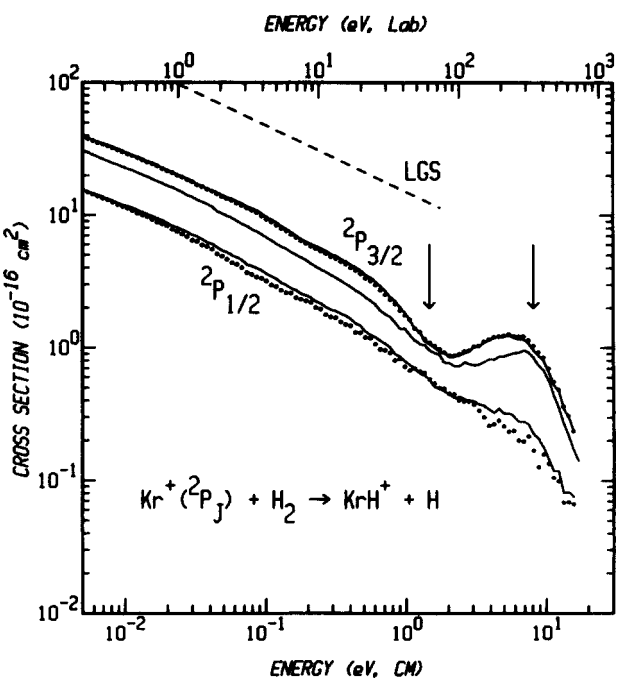

FIG. 5. Spin-orbit state-selected cross sections for reaction (1) plotted as a function of the ion kinetic energy in the laboratory frame (upper scale) and the center-of-mass frame (lower scale). The solid lines represent the experimental data for $Kr^+(^2P_J)$ beams with 96.4 $\pm$ 2% $J = 3/2$ (top), a statistical population of spin-orbit states ($\sim$67% $J = 3/2$, middle), and 95.4 $\pm$ 2% $J = 1/2$ (bottom). The points show these data extrapolated at each energy to pure spin-orbit state cross sections. The broken line gives the collision cross section predicted by the LGS model. The arrows indicate the apparent threshold for the $^2P_{3/2}$ high energy feature (left) and the spectator stripping model critical energy (right).

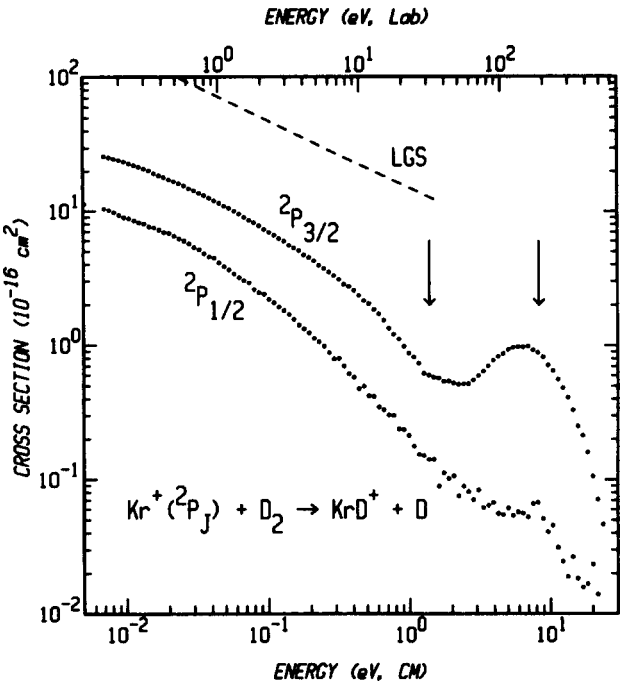

FIG. 6. Spin-orbit state-selected cross sections for reaction (2) plotted as a function of the ion kinetic energy in the laboratory frame (upper scale) and the center-of-mass frame (lower scale). The broken line gives the collision cross section predicted by the LGS model. The arrows indicate the apparent threshold for the $^2P_{3/2}$ high energy feature (left) and the spectator stripping model critical energy (right).

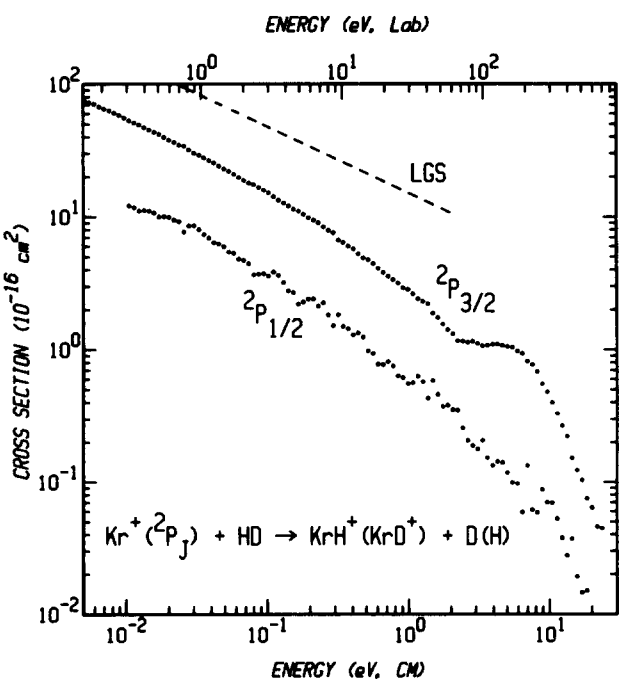

FIG. 7. Spin-orbit state-selected cross sections for reaction (3) plotted as a function of the ion kinetic energy in the laboratory frame (upper scale) and the center-of-mass frame (lower scale). The data are the sum of the KrH^+ and KrD^+ product channels. The broken line gives the collision cross section predicted by the LGS model.

Low energies

At the lowest energies, the $^2P_{3/2}$ ground spin-orbit state reacts about 2.6 times faster with H_2 and with D_2 than does the $^2P_{1/2}$ excited state. For reaction with HD, $\sigma(^2P_{3/2})/\sigma(^2P_{1/2}) \approx 4.2$ below 0.5 eV. Thus, the spin-orbit effect is significantly larger for HD than for either the H_2 or the D_2 reactions.

The energy dependence of the excitation functions of the individual spin-orbit states at low energies is similar but not identical (Figs. 5, 6, and 7). At the lowest energies, the excitation functions for the H_2, D_2, and HD (total) reactions for both spin-orbit levels have approximately the $E^{-1/2}$ dependence predicted by the LGS model. There is no evidence of an activation energy barrier for any of the reactions. At moderately higher energies, the $^2P_{1/2}$ cross section declines somewhat more rapidly with increasing energy for D_2 than for H_2 or HD.

The $^2P_{3/2}$ spin-orbit state exhibits a strong intermolecular isotope effect. At the lowest energies, $\sigma(H_2):\sigma(HD):\sigma(D_2) \approx 1.0:2.0:0.7$ for $Kr^+(^2P_{3/2})$ reactant ions. The LGS model predicts equal cross sections for all three reactions when compared at the same center-of-mass energy. For the $^2P_{1/2}$ state, the intermolecular isotope effect ratio is about 1.0:1.2:0.8 below 0.1 eV. Thus, the unusual intermolecular isotope effect for *statistical* $Kr^+(^2P)$ observed in the cross sections at low energies (Fig. 2) and in the rate constants (Table I) is due largely to the anomalous high reactivity of the $^2P_{3/2}$ spin-orbit state with HD. The intermolecular isotope ratios for the H_2 and D_2 reaction cross sections for either spin-orbit state and for all three isotopic reactions for the $^2P_{1/2}$ state are much smaller.

The intramolecular isotope effect for the $^2P_{3/2}$ ground spin-orbit state is essentially the same as shown in Figs. 3 and 4 for statistical $Kr^+(^2P)$. Due to its much smaller cross section magnitude, the intramolecular branching ratio for the $^2P_{1/2}$ state tends to be obscured by the small fraction of $^2P_{3/2}$ present in the ion beam. Qualitatively, it appears that the intramolecular isotope effect for the $^2P_{1/2}$ spin-orbit state is about the same as for the $^2P_{3/2}$ state below 0.5 eV. At higher energies, the direction of the isotope effect is the same for both spin-orbit states, but the $^2P_{1/2}$ state appears to have a weaker isotope effect (i.e., branching ratios closer to 50%) than the $^2P_{3/2}$ state.

Rate constants derived from these cross sections may be compared to the spin-orbit state-selected thermal rate constant measurements of Futrell and co-workers[21] for reaction (1) and of Adams, Smith, and Alge (ASA)[22] for all three isotopic reactions. These results are presented in Table I. The spin-orbit state-specific rate constants are in reasonably good agreement for reaction (1). For reactions (2) and (3), the present rate constants for the $^2P_{1/2}$ state are in good agreement with ASA, but for the $^2P_{3/2}$ state ASA's rate constants are 60%–70% larger than ours. Thus, the discrepancies noted above for the statistical rate constants are mainly due to the larger value ASA obtain for $^2P_{3/2}$ relative to our results. The ratios of rates for the spin-orbit states also reflect these differences (Table I). The largest deviation is for the HD reaction, where ASA obtain a value of $k(^2P_{3/2})/k(^2P_{1/2}) = 9.4$, compared to our result of ~ 4.2. However,

there is agreement that the spin-orbit state effect is substantially larger for reaction (3) than it is for reactions (1) or (2).

$^2P_{3/2}$ high energy feature

The feature at higher energies in the mixed-state cross sections is shown by the spin-orbit state-selected results to be due *exclusively* to the $^2P_{3/2}$ ground state. The $^2P_{1/2}$ excited state cross sections decline monotonically with increasing energy. This behavior is observed for all three isotopic reactions (Fig. 5, 6, and 7). The pronounced difference in the high-energy behavior of the two spin-orbit states is a striking result. It indicates that not only do the spin-orbit states exhibit different relative probabilities of reaction, but also that they undergo different reaction mechanisms.

The apparently endoergic feature of the $^2P_{3/2}$ state peaks at 1.2 Å^2 at about 5.9 eV for H_2 and at 0.9 Å^2 at about 6.4 eV for D_2. At the peak of the endoergic feature, the $\sigma(^2P_{3/2})/\sigma(^2P_{1/2})$ ratio reaches a maximum of about 15 for D_2 but only about 6 for H_2. This reflects the observation that the $^2P_{1/2}$ cross section for reaction (2) declines more rapidly with increasing energy than for reaction (1). The HD endoergic feature has a different shape than H_2 or D_2 as a result of a strong intramolecular isotope effect in this region. Near the "threshold" for the high-energy feature, the KrD^+ product is very strongly favored, while the peak of the KrH^+ product is shifted to higher energies. The $\sigma(^2P_{3/2})/\sigma(^2P_{1/2})$ ratio for the total cross section with HD reaches a maximum of about 8 at about 5 eV.

Because the high energy features overlap with the lower energy cross sections, it is not possible to extract definitive threshold energies for the apparently endoergic processes. Nevertheless, we can attempt a rough "deconvolution" by extrapolating the declining cross section from lower energies and subtracting that from the total cross section. Figure 8(a) shows the results of this procedure. It should be emphasized that the deconvolution is strictly empirical and somewhat arbitrary. The scatter in the base line below the apparent thresholds gives an indication of the uncertainty involved in the deconvolution procedure. The apparent threshold energies exhibited by these deconvoluted excitation functions are given in Table II and are also indicated by arrows in Figs. 3 to 6. The apparent threshold for the KrD^+ product from HD is less certain than for the other reactions because the feature merges with the low-energy part of the cross section. The shoulder near the threshold for reaction (3b) is probably an artifact of the deconvolution. It is clear however, that the apparent threshold energy for the KrD^+ channel of reaction (3) is much lower than for the KrH^+ channel. The threshold energies for reactions (1) and (2) are the same and are intermediate between the two channels of reaction (3). The peaks of the features exhibit similar energy shifts [Fig. 8(a)]. These energy shifts for the HD product channels are the cause of the extreme intramolecular isotope effects observed above 1 eV (Fig. 4).

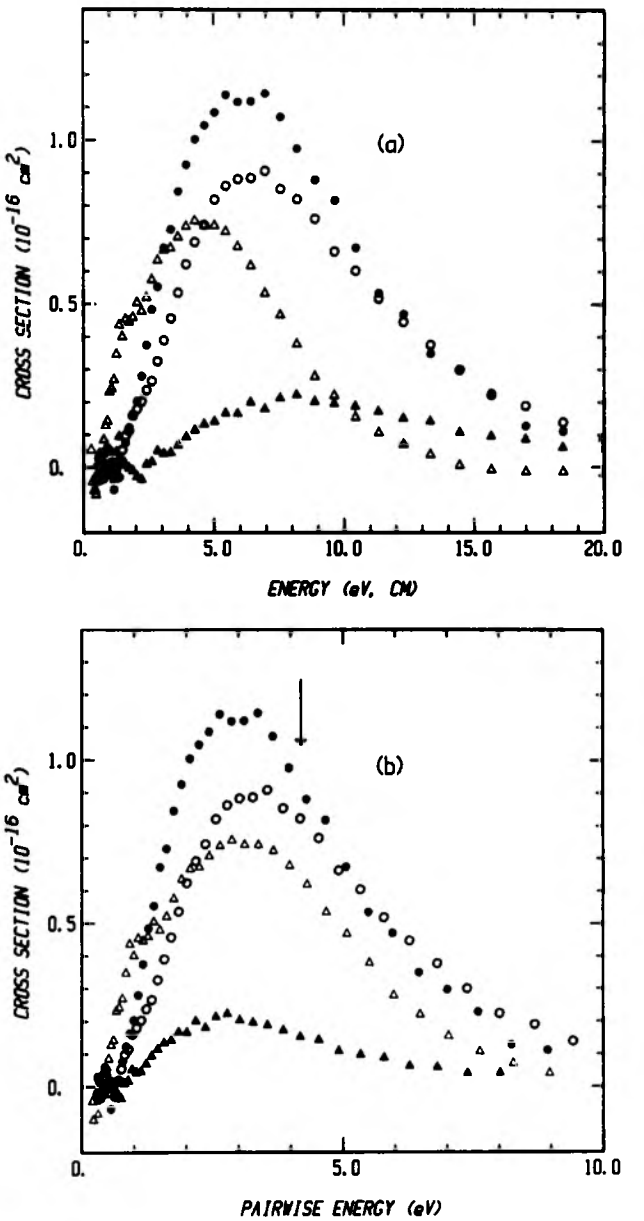

FIG. 8. High energy feature of the $Kr^+(^2P_{3/2})$ cross sections for reactions (1), solid circles; (2), open circles; (3a), solid triangles; and (3b), open triangles. The cross sections are empirically deconvoluted from the low energy cross sections as described in the text. (a) Cross sections as a function of the center-of-mass frame energy; (b) cross sections as a function of the pairwise interaction energy, Eq. (12). The arrow in part (b) indicates the spectator stripping model critical energy (Table II).

DISCUSSION

The pronounced spin-orbit effects and unusual isotope effects apparent in the cross sections for reactions of $Kr^+(^2P_J)$ with H_2, D_2, and HD indicate that the underlying reaction dynamics are complex. A full understanding of these effects requires knowledge of the potential energy surfaces of the KrH_2^+ system including spin-orbit coupling. Quantitative information about these surfaces is limited, but the major features can be pieced together from molecular orbital and electronic state correlations and analogies with other rare gas/hydrogen systems. We will first consider the asymptotic charge states and energetics of the system (in the absence of spin-orbit effects), then molecular orbital and electronic state correlations between reactants and products, and finally the role of spin-orbit coupling.

TABLE II. Threshold and peak energies (eV) of $^2P_{3/2}$ high energy feature.

Reactant (BC)[b]	Threshold		Peak		E_a[a]	
	c.m.[c]	p.w.[d]	c.m.	p.w.	c.m.	p.w.
H_2	1.5 ± 0.2	0.8 ± 0.1	5.9	3.1	8.1	4.1
D_2	1.4 ± 0.2	0.7 ± 0.1	6.4	3.3	8.0	4.1
HD	2.4 ± 0.3	0.8 ± 0.1	8.2	2.8	12.0	4.1
DH	0.7 ± 0.3	0.5 ± 0.2	4.4	3.0	6.1	4.1

[a] Product dissociation threshold.
[b] Atom transferred in reaction is underlined.
[c] Center-of-mass frame energy, Eq. (10).
[d] Pairwise interaction energy, Eq. (12).

Asymptotic $[Kr + H + H]^+$ states

Figure 9 shows the asymptotic potential energy curves[44–46] for $[Kr + H_2]^+$ reactants and $[KrH + H]^+$ products, neglecting spin-orbit coupling. The energy levels of the curves in the $[Kr + H + H]^+$ separated atom limit are offset by the 0.40 eV difference in the ionization potentials of Kr (13.999 eV) and H (13.595 eV).[20] The lowest energy state of reactants is $Kr^+(^2P) + H_2$, which dissociates to $Kr^+ + H + H$. The charge transfer state, $Kr + H_2^+$, lies 1.43 eV above ground state $Kr^+(^2P) + H_2$ and dissociates to $Kr + H^+ + H$. The two curves cross since in the separated atom limit $Kr^+ + H + H$ lies higher than $Kr + H^+ + H$ (Fig. 9). On the product side, the asymptotic dissociation limit for ground state $KrH(^1\Sigma) + H$ is $Kr + H^+ + H$, while the $Kr^+ + H + H$ configuration leads to repulsive excited states of KrH^+. These separated atom limits thus indicate that $Kr^+ + H_2$ reactants correlate diabatically (i.e., while conserving electronic configuration) with the excited product states. Ground state products correlate diabatically with the $Kr + H_2^+$ charge state of reactants.

Figure 10(a) depicts the diabatic electronic state correlations between the asymptotic reactant and product states. Diabatic correlations are drawn as lines connecting the electronic states of reactant (left side) with the electronic states of products (right side). Since there have been no calculations or spectroscopic observations of the excited states of KrH^+, the ordering of those states is uncertain and the correlations are not definitive. The $Kr^+(^2P) + H_2(^1\Sigma)$ reactants probably correlate diabatically with the doublet components of $KrH^+(^3\Sigma,^3\Pi) + H(^2S)$, as shown. Figure 10(a) illustrates that there is no diabatic path between ground state reactants and products. In this simple diabatic correlation scheme, therefore, $Kr^+ + H_2$ reactants cannot form ground state products directly. As Kuntz and Roach originally pointed out,[46] $Kr^+ + H_2$ reactants must cross over to the $Kr + H_2^+$ charge state in order to reach ground state $KrH^+ + H$ products.

Molecular orbital and electronic state correlations

Further examination of the interaction between the asymptotic charge states of $[Kr + H + H]^+$ requires consideration of the electronic structure of the reactants. Mahan[47] has discussed molecular orbital and electronic state correlations for rare gas ion/hydrogen reactions. As $Kr^+[s^2p^5]$ approaches an H_2 molecule approach along the z axis, there are three possible orientations of the p orbital with the lone electron with respect to the H_2 molecule. For convenience, we will use Kuntz and Roach's[46] designation of these orientations as P_x, P_y, and P_z "states," although they

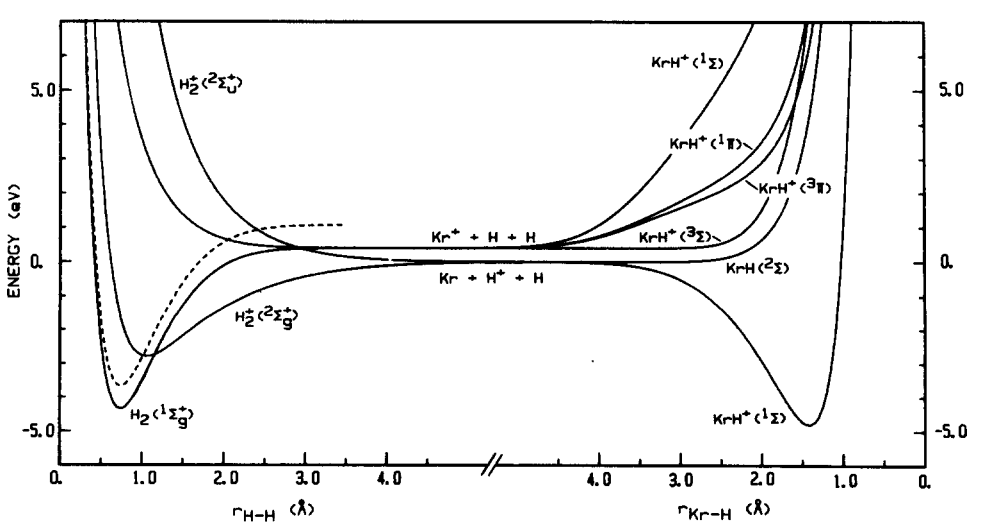

FIG. 9. Schematic asymptotic potential energy curves for the $[Kr + H + H]^+$ system. The curves on the left represent the energies as a function of r(H–H) with r(Kr–H_2) = ∞; the curves on the right represent the energies as a function of r(Kr–H) with r(KrH–H) = ∞. The asymptotic energies shown are for the $Kr^+(^2P_{3/2})$ spin-orbit state; the dashed line shows the potential energy curve for $[Kr^+(^2P_{1/2}) + H_2(^1\Sigma)]$ for comparison.

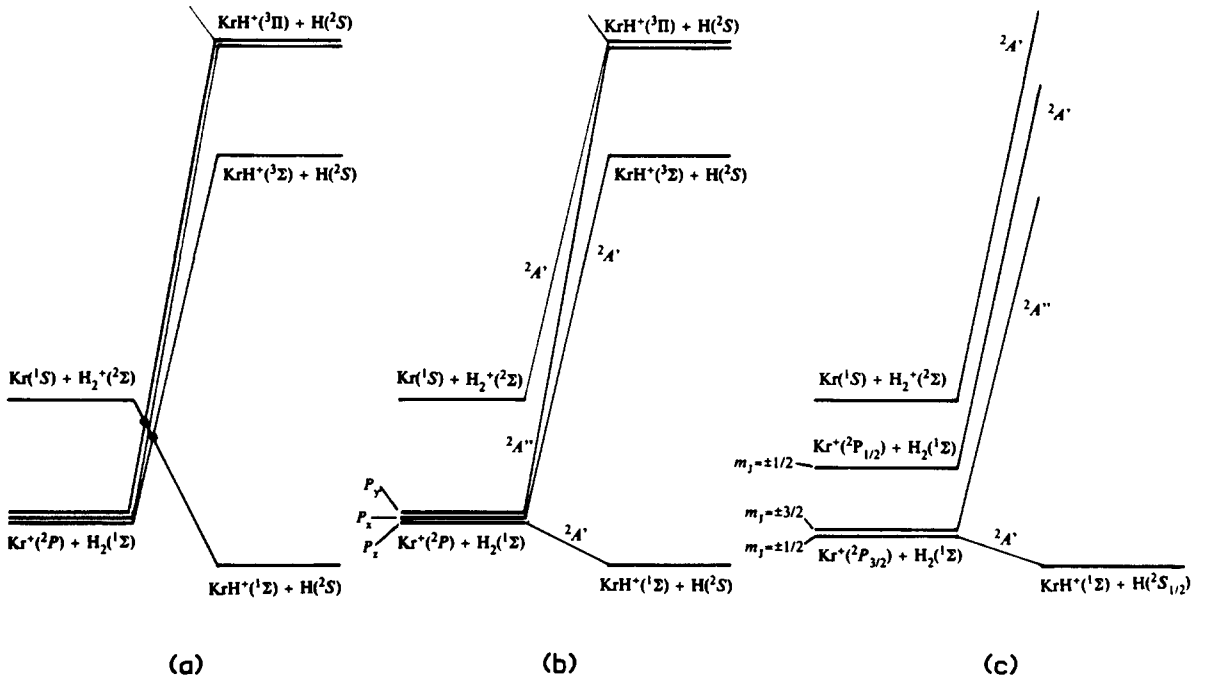

FIG. 10. Electronic state correlation diagrams for reaction (1) in C_s symmetry. The three diagrams show (a) diabatic and (b) adiabatic correlations neglecting spin-orbit coupling, and the (c) adiabatic correlations in the large spin-orbit coupling limit. Energy levels of $[Kr + H_2]^+$ reactant states are shown on the left-hand side of each diagram; $[KrH + H]^+$ product states are on the right. The energy levels are not to scale.

are more properly identified by the M_L and M_S quantum numbers.[48] In the P_z and P_x states, the half-filled p orbital lies in the plane of the three nuclei and is oriented along (P_z) or perpendicular to (P_x) the Kr^+–H_2 axis. In the P_y state, the half-filled p orbital is perpendicular to the plane.

Molecular orbital considerations suggest that the least repulsive orientation of the reactants is a near-collinear P_z approach. This is because the half-filled p_z orbital can mix with the empty σ_u^* antibonding orbital of hydrogen, thus weakening the H–H bond and promoting formation of the KrH^+ bond, while the filled p orbitals are directed away from the line of approach. The P_x and P_y states have a p_z orbital with two electrons, which places three electrons in the KrH^+ bonding orbitals and therefore leads to repulsive excited states of KrH^+.

The P_z and P_x orientations are symmetric with respect to reflection in the plane of the three nuclei and therefore form a $^2A'$ surface in C_s symmetry. P_y is antisymmetric with respect to reflection in the plane and forms a $^2A''$ surface. The $Kr(^1S) + H_2^+(^2\Sigma)$ charge state of reactants and ground state $KrH^+(^1\Sigma) + H(^2S)$ products both form $^2A'$ states, which diabatically correlate with each other. The correlation curves in Fig. 10 are labeled according to the C_s symmetry groups. Crossings of surfaces which have the same symmetry and will therefore be avoided are designated in Fig. 10(a) by circles at the intersections of the diabatic correlation curves. Figure 10(b) shows the resulting adiabatic correlations (still neglecting spin-orbit interactions). Figure 10(b) shows that there is an adiabatic path between ground state reactants and ground state products. Based on the molecular orbital considerations above, we have presumed that it arises from the P_z state. The other two states, $^2A''(P_y)$ and $^2A'(P_x)$, and also the $Kr + H_2^+$ charge state lead adiabatically to repulsive product states.

It should be made clear that the energies of the potential energy surfaces along the reaction path are not known; the correlations in Fig. 10 merely connect reactant and product states of the correct symmetry. The absence of an energy threshold in the experimental cross sections, however, indicates that the lowest adiabatic surface has no overall energy barrier. Apparently, the crossing between the two charge states occurs at an energy below that of ground state $Kr^+ + H_2$ reactants. This is possible since the approach of the reactants is initially attractive due to the r^{-4} ion-induced dipole potential. Since KrH_2^+ is at most weakly bound and the reaction is just 0.3 eV exothermic, it is expected that the lower adiabatic surface is fairly flat along the reaction path.

Kuntz and Roach[46] approximated a potential energy surface for KrH_2^+ by scaling their diatomic-in-molecules (DIM) calculations for ArH_2^+. This surface predicted an energy barrier on the order of 0.4 to 1.2 eV arising from the avoided crossing in the entrance channel for collinear $Kr^+ + H_2$ reactions. The analysis of differential elastic scattering of H_2^+ on Kr by Henglein *et al.*[31(b)] also indicated an energy barrier, ~0.6 eV, for formation of KrH_2^+ from $Kr^+(^2P_{3/2}) + H_2$. The preponderance of experimental evidence since then, both the magnitude of the thermal rate constant[49] and the lack of a threshold in the low-energy cross sections, excludes the possibility of an energy barrier of this magnitude. The failure of the DIM surface is perhaps not too surprising considering it was not calculated explicitly for the KrH_2^+ system. Kuntz and Roach's DIM surface[46] also neglects spin-orbit effects entirely, although it is possible to include spin-orbit coupling in the DIM formulation.[48,50]

Fennelly[42] has pointed out that the validity of the elastic scattering results may be suspect because the results were analyzed with a two-body instead of a three-body potential energy function and because the effect of the charge transfer reaction on the nonreactive scattering was not considered. In light of the correlations shown in Figs. 9(a) and 9(b), however, it is also possible that the elastic scattering is sensitive to the avoided crossings between the $^2A'$ surfaces. If this is the case, the $Kr–H_2^+$ well depth determined by Henglein *et al.*[31(b)] would refer to an excited state surface of KrH_2^+ and not to the ground state surface.

It is interesting to compare the $Kr^+ + H_2$ system with $Ar^+ + H_2$.[25] In the argon reaction, the two charge states have very similar energies and are strongly mixed upon approach of the reactants. The avoided crossing between these diabatic surfaces occurs at large separations of the reactants, 4 to 5 Å, along a seam orthogonal to the H–H vibrational coordinate.[46] Since the $Ar + H_2^+$ charge state has a lower energy asymptotically than the $Ar^+ + H_2$ state, the avoided crossing is accessible to low energy $Ar^+ + H_2(v = 0)$ reactants. Trajectory surface hopping calculations[51] on the ArH_2^+ DIM surface[46] show that $Ar^+ + H_2$ collisions can lead to products directly via the lower surface, or via nonadiabatic transitions between the adiabatic surfaces. Such nonadiabatic transitions are enhanced by vibrational motion in the H–H direction.

In contrast to the argon system, the two $[Kr + H_2]^+$ asymptotic charge states are separated by a much larger energy than in the argon system *and* the $Kr + H_2^+$ state has a higher energy than $Kr^+ + H_2$ reactants (Fig. 9). For krypton, therefore, the asymptotic crossing occurs at a higher energy and at H–H bond distances corresponding to vibrationally excited hydrogen (above $v = 2$ for H_2, $v = 3$ for HD, and $v = 4$ for D_2). Although the energy barrier predicted by the DIM surface does not exist, the coupling of the charge-state surfaces is probably less efficient and more localized compared to the argon system. Thus, there may be steric or dynamic restrictions on reactive trajectories, which would explain the small cross sections relative to the LGS collision cross section at low energies. The reaction $H_2^+ + Kr \rightarrow KrH^+ + H$, on the other hand, is very efficient. Its rate equals or exceeds the LGS collision rate.[21,52] Apparently, the diabatic path from $Kr + H_2^+$ to products [Fig. 10(a)] is very efficient.

Spin-orbit effects

Assuming that the three degenerate states of reactants are populated statistically, only one-third of the initial collisions of reactants will end up on the adiabatic surface leading to ground state products [Fig. 10(b)]. Nonadiabatic transitions between the surfaces are also possible, but before considering such effects it is desirable to discuss the role of spin-orbit coupling.

The excited $^2P_{1/2}$ spin-orbit state of Kr^+ lies about halfway between the $^2P_{3/2}$ ground state and the charge transfer state, as shown by the dashed potential energy curve in Fig. 9. The asymptotic crossing with the $Kr + H_2^+$ charge state occurs at a lower energy relative to reactants for $^2P_{1/2}$ than for $^2P_{3/2}$. This energy effect alone might be expected to cause a difference in behavior for the two spin-orbit states. A naive conclusion would be that it would be easier for the $^2P_{1/2}$ state to cross over to the $Kr + H_2^+$ state, which then leads diabatically to products. That, however, is contrary to the experimental result that the lower spin-orbit state is more reactive at all energies than the upper spin-orbit state.

Two spin-orbit coupling schemes will be considered: the small spin-orbit limit and the large spin-orbit limit.[53] Dagdigian and co-workers[12] have recently discussed related considerations in their work on spin-orbit state-specific reactions of $Ca(^3P_J)$. In the *small* spin-orbit coupling limit, molecular orbital (electrostatic) interactions between the ion and approaching hydrogen molecule exceed the spin-orbit interaction. In this case, the orientational effects discussed above would remain important—namely, only the P_z approaches would react. Spin-orbit coupling, however, mixes the P_x, P_y, and P_z states. Instead of being equally likely, the flux to the $^2A'(P_z)$, $^2A''(P_y)$, or $^2A'(P_x)$ surface depends on the initial spin-orbit state of the reactant ion. Table III gives the correspondence between the asymptotic spin-orbit states and the linear combinations of the $KrHH^+$ states.[19,48] Neglecting possible mixing among the $^2P_{J,m_J}$ states, the resulting flux from each spin-orbit state to the P_z state is $(2/3)^{1/2}$ for $^2P_{3/2,\pm 1/2}$, none for $^2P_{3/2,\pm 3/2}$, and $(1/3)^{1/2}$ for $^2P_{1/2,\pm 1/2}$. Assuming only the P_z orientation reacts, the $^2P_{1/2}$ reactivity is enhanced by a factor of $2^{1/2}$ or about 40% over that of $^2P_{3/2}$. This argument was used in a model developed by Koyano and co-workers[19] to explain their spin-orbit state-selected cross section results for the $Ar^+(^2P_J) + H_2$ and D_2 reactions. The result is in qualitative agreement with the experimental results for $Ar^+(^2P_J) + H_2$ and D_2, for which the spin-orbit splitting is 0.17 eV, but is in the wrong direction for the present results for $Kr^+ + H_2$. The relatively large spin-orbit splitting for Kr^+, 0.67 eV, means that the small spin-orbit coupling limit may not be applicable.

In the *large* spin-orbit coupling limit,[54] the spin-orbit

TABLE III. Asymptotic electronic states and energy levels.

Asymptotic state	$KrHH^+$ state	C_s symmetry	Energy (eV)
$Kr^+(^2P_{3/2,\pm 1/2}) + H_2(^1\Sigma)$	$\sqrt{1/6}(P_x \pm P_y) + \sqrt{2/3}P_z$	$^2A'$	0.0
$Kr^+(^2P_{3/2,\pm 3/2}) + H_2(^1\Sigma)$	$\sqrt{1/2}(P_x \pm P_y)$	$^2A''$	0.0
$Kr^+(^2P_{1/2,\pm 1/2}) + H_2(^1\Sigma)$	$\sqrt{1/3}(P_x \pm P_y) - \sqrt{1/3}P_z$	$^2A'$	0.67
$Kr^+(^1S) + H_2^+(^2\Sigma)$		$^2A'$	1.43
$KrH^+(^1\Sigma) + H(^2S_{1/2,\pm 1/2})$		$^2A'$	−0.29

coupling is comparable to or larger than the molecular orbital interactions of the approaching reactants. In this case, the electronic states are mixed by the spin-orbit coupling in all regions of configuration space, creating new adiabatic electronic surfaces. Since the adiabatic correlations between reactants and products for these new surfaces differ, the initial spin-orbit states of the reactants strongly influence the products or product states formed in a reaction. Figure 10(c) shows the adiabatic electronic state correlations including spin-orbit coupling. The $m_J = \pm 1/2$ components of the $^2P_{3/2}$ state correlate with the lowest $^2A'$ state upon approach of H_2, while the $m_J = \pm 3/2$ components correlate with the $^2A''$ state. The excited $^2P_{1/2}$ spin-orbit state of krypton has only $m_J = \pm 1/2$ components and correlates with the upper $^2A'$ state. Ground state products $KrH^+(^1\Sigma) + H(^2S_{1/2})$ have $m_J = \pm 1/2$ and correlate with the $^2A'$ state emanating from $Kr^+(^2P_{3/2,\pm 1/2}) + H_2$. The $^2P_{3/2,\pm 3/2}$ and $^2P_{1/2,\pm 1/2}$ spin-orbit levels lead adiabatically to excited products.

Reaction mechanisms

The adiabatic correlations in Fig. 10(c) allow several conclusions to be drawn regarding the relative reactivity of the spin-orbit states. If the reactants are initially on the lowest-energy $^2A'$ surface, ground state products can be formed directly along the adiabatic surface. This reaction pathway can account for the reactivity of $Kr^+(^2P_{3/2})$ at low energies. Statistically, 50% of the incident $^2P_{3/2}$ ions (those with $m_J = \pm 1/2$) would be on this surface. The experimental $^2P_{3/2}$ cross sections are 20% of LGS for H_2, 13% for D_2, and 29% for HD. The observation that the cross sections are significantly smaller than 50% of the LGS collision cross section probably indicates that there are further dynamic constrictions along the reaction path. This could be the case if only certain orientations are able to reach the barrierless pathway to the avoided crossing with the $Kr + H_2^+$ charge state. Hierl's differential cross secton results up to 1 eV (which our spin-orbit state-selected cross sections show are about 75% due to the $^2P_{3/2}$ spin-orbit state) indicate that the reaction proceeds mainly by low-impact parameter, hard-sphere like collisions. This is consistent with the molecular orbital considerations which indicate that collinear approaches may be favored.

If the reactants are initially on the second $^2A'$ surface originating from $Kr^+(^2P_{1/2}) + H_2$, ground state products can be formed only via nonadiabatic transitions to the lower surface. Nonadiabatic transitions between surfaces of the same symmetry (i.e., $^2A'$ to $^2A'$) can be induced by the motion of the nuclei (translational, vibrational, or rotational). Details of the two $^2A'$ surfaces are not known in the present case, but the interaction between them may be sufficient to allow nonadiabatic transitions from the upper surface down to the reactive surface. In-plane rotational motion of the H_2 can induce such nonadiabatic transitions by mixing the P_z and P_x states, for which the p orbitals with the unpaired electrons lie in the plane. The $^2P_{1/2}$ spin-orbit state already has components of the P_x and P_z states (Table III). This nonadiabatic transition mechanism could be responsible for the reaction of the $Kr^+(^2P_{1/2})$ spin-orbit state at low energies. It is consistent with the observation of a relatively small reaction probability for this process, about 6% to 8% of LGS below 0.5 eV. This suggests that the transition probability is low but significant. The observation that the $^2P_{1/2}$ cross section has approximately the $E^{-1/2}$ energy dependence predicted by the LGS collision model implies that this nonadiabatic transition probability is independent of kinetic energy at low energies.

The $^2A''$ state of reactants, which emanates from $Kr^+(^2P_{3/2,\pm 3/2}) + H_2$, cannot undergo ordinary nonadiabatic transitions to the reactive $^2A'$ surface. Physically this is because the out-of-plane orbital responsible for the A'' symmetry cannot mix with the in-plane orbitals via nuclear motion in the plane of the three nuclei. The only mechanism for transitions from A'' to A' symmetry is Coriolis or rotationally nonadiabatic coupling.[55] This can occur when high rotational velocities of the collision plane of the reactants cause the electrons to "lag" out of the plane.[56] Coriolis coupling is proportional to r^{-2}, where r is the distance of closest approach.[55] Since r decreases with increasing collision energy, Coriolis coupling effects may appear as a process with an activation energy.[56]

We hypothesize that nonadiabatic transitions induced by Coriolis coupling is the mechanism responsible for the high energy feature of the $Kr^+(^2P_{3/2})$ cross sections. The experimental evidence is largely circumstantial: (1) The $^2P_{3/2}$ state exhibits two distinct features while the $^2P_{1/2}$ state shows only one. This suggests that the two m_J components of the $^2P_{3/2}$ state might be responsible for different behavior. (2) The high energy feature clearly has an apparent activation barrier. As discussed above, this could be the result of a Coriolis coupling effect. (3) The impulsive reaction dynamics evident from the isotope effects (discussed further below) is consistent with a process that occurs only at high velocities and small impact parameters. Other possible explanations for the high-energy $^2P_{3/2}$ feature can be excluded: (1) There are no excited state product channels accessible at energies low enough to account for the apparent threshold energy of the feature, even allowing for radiative transitions to the ground state. (2) An impulsive reaction process which manifests an apparent energy barrier (say, sequential collisions or a knockout process) is a conceivable explanation for the high energy process, but a strong spin-orbit state dependence would not be expected for a solely dynamic effect. These considerations lead us to believe that Coriolis coupling is a reasonable explanation for the observed endoergic feature. Theoretical work will be required to determine whether the approximate 1 eV apparent activation energy is sufficient or appropriate for Coriolis-induced transitions and whether the transition probability would be sufficient to explain the magnitude of the cross sections.

Intramolecular isotope effect at low energies

An orientation isotope effect model was developed by Hierl[32] to explain the branching ratio of reaction (3) at low and intermediate energies. The basic assumption of the model is that the atom transferred is the one that is directed towards the ion when the system surmounts the centrifugal barrier on the ion-induced dipole potential or when it crosses

to the $Kr^+ + HD$ charge state. The orientation probability is influenced by the collision energy, the HD rotational energy, and the torque exerted on HD by the ion due to the displacement of the center-of-polarizability from the center-of-mass of HD. The branching ratio predicted by the orientation isotope effect model is plotted in Fig. 4 for comparison with the data. The agreement, although not quantitative, is quite good considering the simple assumptions employed in the model. The model predicts a much weaker isotope effect for the $Ar^+ + HD$ reaction, which is in qualitative agreement with the experimental results.[25] The main difference between the two systems is that the crossing to the other charge state of reactants occurs at much larger distances for argon. This gives $Kr^+ + HD$ a longer time to orient in the model.

At very low energies, the orientation isotope model predicts that the deuteride product should be favored, although it strictly breaks down when there is enough time for reorientation after crossing the centrifugal barrier. An alternative explanation of favoring the deuteride product at low energies is statistical behavior of the system. This is because the KrD^+ vibrational and rotational levels are more closely spaced than those of KrH^+. The $Kr^+ + HD$ system does not have a deep well to support a very long-lived intermediate, but the collision complex may last for several vibrational periods. This may be all that is required for statistical behavior. A simple statistical treatment[57] predicts $\sigma(KrH^+)/\sigma(KrD^+) \approx 2^{-1/2}$ or a branching ratio of 41.4% KrH^+. This is in reasonable agreement with the experimental value of ~46% KrH^+ at the lowest energies.

Intermolecular isotope effect at low energies

The intermolecular isotope effect at low energies is an intriguing phenomenon, particularly the $\alpha(HD) > \sigma(H_2) > \sigma(D_2)$ ordering. The electronic potential energy surfaces are the same for reactions (1), (2), and (3). The primary mass effect is the difference in relative energies for a given velocity of reactants for the three isotopic systems. This effect is taken into account by the conversion of the data to relative (center-of-mass frame) energies according to Eq. (10). Secondary mass effects can be due to the different vibrational and rotational energy levels and spacings of H_2, HD, and D_2 and of the KrH^+ and KrD^+ products. In a process that behaves statistically, the formation of a particular channel depends on the density of states. However, the density of rotational and vibrational states increases from H_2 to HD to D_2, so this argument cannot explain the observed isotope dependence.

Symmetry effects represent another possibility to account for the intermolecular isotope effect. Since HD is heteronuclear, the $Kr^+ + HD$ reactants have lower symmetry in perpendicular configurations than $Kr^+ + H_2$ or D_2. However, these reactions are expected to favor collinear approaches, where there is no difference in symmetry group. Neither is there a difference in C_s configurations.

An energy resonance between specific vibrational/rotational levels of two reactant channel charge states could enhance transitions between the two states. In the krypton system there are no close resonances between asymptotic vibrational states (with zero rotational energy) for reactions (1), (2), and (3) for either spin-orbit state. In fact, the energy defects are largest for the HD system, which has the largest cross section. Furthermore, the $Kr + H_2^+$ charge state is 1.43 eV higher in energy than $Kr^+ + H_2$ reactants, so asymptotic energy resonances can play no role at low collision and vibrational energies. It is possible that vibrational or rotational resonances influence transitions between surfaces at closer separations of the reactants. Not enough is known about the potential energy surfaces to warrant speculation on this point.

A final possible explanation for the larger HD cross sections involves the displacement of the center-of-mass from the center-of-polarizability in HD. As Hierl discussed in his orientation model for the intramolecular isotope effect,[32] this displacement causes the ion-induced dipole attractive force to exert a torque on the HD molecule. This anisotropy of the potential energy surface could couple rotational and electronic degrees of freedom in the entrance channel of reaction (3) and thus influence the ability of the $Kr^+ + HD$ reactants to pass through the avoided crossing with the $KR + HD^+$ charge state. This interaction is absent in the reactions of homonuclear H_2 and D_2.

Isotope effects at high energies

In the region of the $^2P_{3/2}$ high energy feature, the extreme intramolecular isotope effects (Fig. 4) indicate that the reaction mechanism is direct and impulsive. Extreme isotope effects similar to these have been seen in other systems recently in our laboratory. Specifically, the reactions $Mn^+(^7S)$,[58] $Fe^+(^6D)$,[59] and $He^+(^2S)$ and $Ne^+(^2P)$[60] with HD also show the general behavior that the deuteride product is very strongly favored near the threshold of a process and the hydride appears at higher energies if at all. As in the present case, the apparent threshold energies for the reactions with H_2 and D_2 are the same, but fall at an energy intermediate between the thresholds of the two channels for reaction with HD. These reactions have an additional common denominator—they all exhibit activation barriers to reaction which can be explained by electronic structure considerations. This isotope behavior can be understood by an impulsive reaction mechanism in which the atoms interact in a pairwise fashion. The energy available to binary atomic interactions depends on the mass of the atom the ion first encounters. For a general reaction $A + BC \rightarrow AB + C$, where the primary interaction is between atoms A and B, the conversion between the true center-of-mass frame energy E_{cm} and the pairwise energy E_P is given by [59]

$$E_P = E_{c.m.} \cdot M \cdot m_B/(m_A + m_B) \cdot (m_B + m_C), \quad (12)$$

where m_i refers to the mass of atom i and $M = m_A + m_B + m_C$. The pairwise interaction energy is always less than $E_{c.m.}$. For heavy atomic reactants, $m_A \gg m_B$ and $m_A \gg m_C$, E_P is approximately 1/2, 1/3, 2/3, and 1/2 $E_{c.m.}$ for reaction with H_2, HD (B = H), HD (B = D), and D_2, respectively. Thus, for a pairwise interaction the available energy for the individual channels of the HD reaction is very different from each other and from H_2 and D_2.

The $^2P_{3/2}$ high-energy features, deconvoluted as de-

scribed in the results section, are plotted on the pairwise energy scale in Fig. 8(b). Table II compares the apparent threshold and peak energies on the center-of-mass and pairwise energy scales. For reaction with HD, it is assumed that atom B in Eq. (12) is the atom transferred in the reactions. These comparisons demonstrate that the apparent thresholds *and* peaks for the $^2P_{3/2}$ high energy feature of reactions (1), (2), and (3) all coincide on the pairwise energy scale. [The threshold for reaction (3b) is a possible exception, but as noted in the Results section the "deconvolution" of this channel is very uncertain.] This correspondence supports the hypothesis of a pairwise atomic interaction mechanism.

Above a certain collision energy, the nascent product diatom can acquire excess internal energy and subsequently dissociate. The thermochemical threshold for the lowest-energy dissociation reaction, $Kr^+ + H_2 \rightarrow Kr + H^+ + H$, is 4.1 eV. If this energy must be supplied in a pairwise interaction process, Eq. (12) gives the corresponding center-of-mass frame energy required for product dissociation. This energy, E_s, is listed for each reaction channel in Table II and is indicated by arrows in Figs. 3, 4, 5, 6, and 8(b). KrH^+ formation should decline with the onset of product dissociation, and in fact E_s lies just slightly above the peaks of the high-energy feature for reactions (1), (2), (3a), and (3b).

E_s is identically equal to the critical product dissociation energy in the familar spectator stripping model. Spectator stripping is a special case of pairwise impulsive behavior in which additional assumptions are made regarding the distribution of product translational and internal energies. In true spectator stripping, the cross sections would fall to zero at the critical energy. The formation of products above the critical energy indicates that more energy goes into product translation than predicted in the extreme stripping limit. Measurements of the differential reactive scattering cross sections for HD would further elucidate the reaction dynamics of the high-energy process. Unfortunately, the differential cross sections results[30] only extend up to 3 eV c.m. They do show increasing impulsive behavior at the higher energies studied. There is still substantial wide-angle scattering,[30] which also indicates that more energy is distributed into translational modes than in the stripping model.

Is the Coriolis coupling effect used to explain the existence of the $^2P_{3/2}$ high energy process compatible with the pairwise, impulsive reaction mechanism proposed here? Theoretical calculations may be required to answer this question definitively. Nevertheless, it seems reasonable that high velocity, low impact parameter collisions which lead to close approaches of the reactants and Coriolis-induced transitions to the reactive electronic surface would also exhibit the very impulsive reaction dynamics which are indicated by the isotope effects of the high energy feature.

SUMMARY

Spin-orbit state-selected cross sections have been measured for the hydrogen atom transfer reactions of $Kr^+(^2P_J)$ with H_2, D_2, and HD. At low energies the ground $^2P_{3/2}$ spin-orbit state reacts about 2.6, 2.6, and 4.2 times faster than the excited $^2P_{1/2}$ spin-orbit level for H_2, D_2, and HD, respectively. A process with an apparent activation energy of about 1 eV is observed *exclusively* for the $^2P_{3/2}$ spin-orbit state.

These results have been provisionally explained in terms of adiabatic correlations of the electronic states of the reactants and products and by nonadiabatic coupling mechanisms between the states. The $m_J = \pm 1/2$ components of ground $^2P_{3/2}$ spin-orbit state correlate adiabatically to ground state products, while the $m_J = \pm 3/2$ components lead adiabatically to repulsive, excited products. The experimental results show that the $^2P_{3/2}$ state reacts without a barrier at low energies, but at less than 1/3 the collision cross section. The small reaction probability is partly due to the nonreactivity of the $m_J = \pm 3/2$ component of the $^2P_{3/2}$ spin-orbit level at low energies. In order to reach ground state products, the $Kr^+ + H_2$ reactants must pass through an avoided crossing with the $Kr + H_2^+$ charge state in the entrance channel. Molecular orbital considerations suggest near-collinear and low impact parameter collisions are favored in the coupling of these surfaces. These orientational effects may further reduce the reaction probability.

The $^2P_{1/2}$ upper spin-orbit level of krypton ion reactant does not correlate with ground state products, but nonadiabatic transitions induced by nuclear motion may allow reaction. This accounts for the small cross section for this state (6% to 8% of the collision cross section). The $m_J = \pm 3/2$ components of the ground spin-orbit cannot undergo normal nonadiabatic transition to the reactive state because they are of different symmetry (A'' vs A'). The high-energy feature of the $^2P_{3/2}$ cross section may be due to reaction of the $^2A''$ state via rotational nonadiabatic or Coriolis transitions to the $^2A'$ state.

The $Kr^+ + H_2$ reaction system exhibits strong inter- and intramolecular isotope effects. At low energies, it may be possible to understand the intramolecular isotope effect by statistical or orientational models. The intermolecular isotope effect arises primarily from the observed enhanced reaction probability of the $^2P_{3/2}$ state with HD at low energies. The origin of this intermolecular isotope effect is uncertain. In the region of the $^2P_{3/2}$ high energy feature, extreme inter- and intramolecular isotope effects suggest the reaction mechanism involves impulsive, pairwise interactions between the atoms.

The reactions studied here display a number of intriguing features, including strong spin-orbit effects and unusual isotope effects. We hope these results will encourage theoretical work on this system.

ACKNOWLEDGMENTS

We thank F. Klein for bringing the high-energy feature in the cross sections to our attention. We are indebted to J. Tully for a helpful discussion of Coriolis coupling effects. This research was supported by the National Science Foundation, Grant No. CHE-8306511.

[1]For example, see R. B. Bernstein, *Atom–Molecule Collision Theory* (Plenum, New York, 1979).
[2]K. Bergmann, S. R. Leone, and C. B. Moore, J. Chem. Phys. **63**, 4161 (1975).
[3]J. R. Wiesenfeld and G. L. Wolk, J. Chem. Phys. **69**, 1797,1805 (1978).

[4]P. L. Houston, Chem. Phys. Lett. **47**, 137 (1977).
[5]J. W. Hepburn, K. Liu, R. G. Macdonald, F. J. Northrup, and J. C. Polanyi, J. Chem. Phys. **75**, 3353 (1981).
[6]H. K. Haugen, E. Weitz, and S. R. Leone, Chem. Phys. Lett. **119**, 75 (1985).
[7]R. J. Donovan, F. G. M. Hathorn, and D. Husain, Trans. Faraday Soc. **64**, 1228 (1968).
[8]P. Das, T. Venkitachalam, and R. Bersohn, J. Chem. Phys. **80**, 4859 (1984).
[9]W. Felder and A. Fontijn, J. Chem. Phys. **69**, 1112 (1978).
[10]T. D. Dreiling and D. W. Setser, J. Chem. Phys. **79**, 5423 (1983).
[11]M. F. Golde and Y.-S. Ho, J. Chem. Phys. **82**, 3160 (1985); J. Balamuta, M. F. Golde, and A. M. Moyle, *ibid.* **82**, 3169 (1985); M. F. Golde and R. A. Poletti, Chem. Phys. Lett. **80**, 23 (1981); D. Lin, Y. C. Yu, and D. W. Setser, J. Chem. Phys. **81**, 5830 (1984).
[12]H.-J. Yuh and P. J. Dagdigian, J. Chem. Phys. **81**, 2375 (1984); N. Furio, M. L. Campbell, and P. J. Dagdigian, *ibid.* **84**, 4332 (1986).
[13]R. C. Amme and P. O. Haugsjaa, Phys. Rev. **165**, 63 (1968).
[14]B. Friedrich, W. Trafton, A. Rockwood, S. L. Howard, and J. H. Futrell, J. Chem. Phys. **80**, 2537 (1984); A. L. Rockwood, S. L. Howard, D. Wen-Hu, P. Tosi, W. Lindinger, and J. H. Futrell, Chem. Phys. Lett. **114**, 486 (1985).
[15]L. Hüwel, D. R. Guyer, G. H. Lin, and S. R. Leone, J. Chem. Phys. **81**, 3520 (1984).
[16]T. Kato, K. Tanaka, and I. Koyano, J. Chem. Phys. **77**, 337 (1982).
[17]C. L. Liao, R. Xu, and C. Y. Ng, J. Chem. Phys. **84**, 1948 (1986).
[18]W. A. Chupka and M. E. Russell, J. Chem. Phys. **49**, 5426 (1968).
[19]K. Tanaka, J. Durup, T. Kato, and I. Koyano, J. Chem. Phys. **73**, 586 (1981); **74**, 5561 (1981).
[20]C. E. Moore, *Atomic Energy Levels*, Natl. Stand. Ref. Data Ser. Natl. Bur. Stand. No. 35 (U. S. GPO, Washington, D. C., 1971).
[21]R. D. Smith, D. L. Smith, and J. H. Futrell, Chem. Phys. Lett. **32**, 513 (1975); Int. J. Mass Spectrom. Ion Phys. **19**, 395 (1976).
[22]N. G. Adams, D. Smith, and E. Alge, J. Phys. B **13**, 3235 (1980).
[23]T. T. C. Jones, K. Birkinshaw, J. D. C. Jones, and N. D. Twiddy, J. Phys. B **15**, 2439 (1982).
[24]Reaction enthalpies are derived from the experimental proton affinity of krypton, $PA_{298}(Kr) = 101.6 \pm 3$ kcal/mol [S. G. Lias, J. Liebman, and R. D. Levin, J. Phys. Chem. Ref. Data **13**, 695 (1984)], corrected to 0 K to give $D_0^\circ(Kr\text{–}H^+) = 4.37 \pm 0.06$ eV; spectroscopic values for the bond energy of hydrogen $D_0^\circ(H_2) = 4.4781$ eV [K. P. Huber and G. Herzberg, *Constants of Diatomic Molecules* (Van Nostrand Reinhold, New York, 1979)]; and tabulated ionization potentials [H. M. Rosenstock, K. Draxl, B. W. Steiner, and J. T. Herron, J. Phys. Chem. Ref. Data **6**, Suppl. 1 (1977)]. A theoretical value for the product bond energy, $D_0^\circ(Kr\text{–}H^+) = 4.65 \pm 0.05$eV [P. Rosmus and E.-A. Reinsch, Z. Naturforsch. Teil A **35**, 1066 (1980)], gives an enthalpy value of $\Delta H_0^\circ = -0.57 \pm 0.05$ eV for reaction (1).
[25]K. M. Ervin and P. B. Armentrout, J. Chem. Phys. **83**, 166 (1985); see citations therein for other works on the $Ar^+ + H_2$ system.
[26]W. A. Chupka, in *Interactions between Ions and Molecules*, edited by P. Ausloos (Plenum, New York, 1975), p. 249.
[27]W. A. Chupka and M. E. Russell, J. Chem. Phys. **49**, 5426 (1968).
[28]G. Gioumousis and D. P. Stevenson, J. Chem. Phys. **29**, 294 (1958).
[29]P. R. Kemper, P. V. Neilson, D. Parent, and M. T. Bowers, J. Chem. Phys. **68**, 322 (1978).
[30]J. R. Wyatt, L. W. Strattan, and P. M. Hierl, J. Chem. Phys. **65**, 1593 (1976); S. Chivalak and P. M. Hierl, *ibid.* **67**, 4654 (1977); Chem. Phys. Lett. **45**, 99 (1977).
[31](a) G. Bosse, A. Ding, and A. Henglein, Z. Naturforsch. Teil A **26**, 932 (1971); (b) A. Henglein, J. Phys. Chem. **76**, 3883 (1972).
[32]P. M. Hierl, J. Chem. Phys. **67**, 4665 (1977).
[33]F. Klein, Proc. Am. Soc. Mass Spectrom., Boston, 1983, p. 97. In Figs. 2 and 3 of this abstract, the cross section scales should be multiplied by a factor of 10 [F. Klein (private communication)].
[34]P. A. M. VanKoppen, P. R. Kemper, A. J. Illies, and M. T. Bowers, Int. J. Mass Spectrom. Ion Proc. **54**, 263 (1983).
[35]K. M. Ervin and P. B. Armentrout, J. Chem. Phys. **84**, 6738 (1986).
[36]P. R. Kemper and M. T. Bowers, Int. J. Mass Spectrom. Ion Phys. **52**, 1 (1983).
[37]J. R. Wyatt, L. W. Strattan, and P. M. Hierl, J. Phys. Chem. **80**, 2911 (1976).
[38]K. M. Ervin and P. B. Armentrout (unpublished results).
[39]I. Wendel, R. A. Friedel, and M. Orchin, J. Am. Chem. Soc. **71**, 1140 (1949).
[40]P. J. Chantry, J. Chem. Phys. **55**, 2746 (1971); C. Lifshitz, R. L. C. Wu, T. O. Tiernan, and D. T. Terwilliger, *ibid.* **68**, 247 (1978).
[41]This agreement tends to uphold the rather large correction factors (1.01 to 2.29) used in Ref. 30 to compensate for differences in collection efficiencies at different angles and energies.
[42]P. F. Fennelly, Ph.D. thesis, Brandeis University, 1972 (University Microfilms, Ann Arbor, Mich., No. 72-32095); Paul F. Fennelley, M. J. Henchman, A. S. Werner, and J. F. Paulson (unpublished).
[43]At this low nominal energy, it is important to take into account the experimental energy distributions for comparison to other experiments. According to Eq. (11), $E_{c.m.} = 0.030$ eV corresponds to a mean relative energy $\langle E \rangle = 0.068$ eV.
[44]The potential energy curve for ground state $KrH^+(^1\Sigma)$ is taken from calculations by Rosmus and Reinsch (Ref. 45). There have been no calculations or observations of excited states of KrH^+. The curves in Fig. 9 are scaled versions of the ArH^+ states, as used by Kuntz and Roach (Ref. 46) in their approximate diatomics-in-molecules (DIM) surface for KrH_2^+. None of the excited states arising from ground states of the separated atoms are expected to be bound.
[45]P. Rosmus and E.-A. Reinsch, Z. Naturforsch. Teil A **35**, 1066 (1980).
[46]P. J. Kuntz and A. C. Roach, J. Chem. Soc. Faraday Trans. 2 **68**, 259 (1972).
[47]B. H. Mahan, J. Chem. Phys. **55**, 1436 (1971); Acc. Chem. Res. **8**, 55 (1975).
[48]J. C. Tully, J. Chem. Phys. **60**, 3042 (1974).
[49]P. F. Fennelly, J. D. Payzant, R. S. Hemsworth, and D. K. Bohme, J. Chem. Phys. **60**, 5115 (1974).
[50]J. C. Tully, J. Chem. Phys. **59**, 5122 (1973).
[51]S. Chapman and R. K. Preston, J. Chem. Phys. **60**, 650 (1974); S. Chapman, *ibid.* **82**, 4033 (1985).
[52]K. R. Ryan and I. G. Graham, J. Chem. Phys. **59**, 4260 (1973).
[53]G. Herzberg, *Molecular Spectra and Molecular Structure. I. Spectra of Diatomic Molecules* (Van Nostrand, Princeton, 1950).
[54]J. T. Muckerman and M. D. Newton, J. Chem. Phys. **56**, 3191 (1972).
[55]H. Laue, J. Chem. Phys. **46**, 3034 (1967).
[56]J. C. Tully (private communication).
[57]B. S. Rabinovitch and D. W. Setser, Adv. Photochem. **3**, 1 (1964).
[58]J. L. Elkind and P. B. Armentrout, J. Chem. Phys. **84**, 4862 (1986).
[59]J. L. Elkind and P. B. Armentrout, J. Phys. Chem. (in press).
[60]K. M. Ervin and P. B. Armentrout (to be published).